International Journal of Thin Films Science and Technology

http://dx.doi.org/10.18576/ijtfst/120304

Influence of Effective Surface Area on Gas Sensing Properties and Surface Morphology of Ag Doped Cu_2O Thin Films by Cost Effective Method of M-SILAR Technique

A. Vasuhi[1], K. Dhanabalan[2,], A. T. Ravichandran[3], R. Chandramohan[4], K. Ravichandran[5], R. Shalini[5], and Srinivas Mantha[6]*

[1] PG and Research Department of Physics, H.H. The Rajah's College, Bharathidasan University, Pudukkottai, Tamil Nadu, India- 622 001
[2] PG and Research Department of Physics, J.J. College of Arts and Science, Bharathidasan University, Pudukkottai, Tamil Nadu, India -622 422
[3] PG and Research Department of Physics, National College, Bharathidasan University, Tiruchirappalli, Tamil Nadu, India- 620 001
[4] Department of Mathematics and Physical Science, Nachiappa Swamigal Arts and Science College, Koviloor, Karaikudi, Tamil Nadu, India - 630307
[5] PG and Research Department of Physics, A.V.V.M. Sri Pushpam College, Bharathidasan University, Poondi, Thanjavur, India - 613 503
[6] Department of Electronics & Communication Engineering, SAGE University, Bhopal, India - 462 022.

Received: 12 Mar. 2023, Revised: 07 Apr. 2023, Accepted: 16 Aug. 2023.
Published online: 1 Sep. 2023.

Abstract: Undoped and silver (Ag) doped Cu_2O ($Cu_{2-x}Ag_xO$; x= 2.5, 5.0, 7.5 and 10.0 mol. %) thin films were deposited onto glass substrate using modified successive ionic layer adsorption and reaction (M-SILAR) technique. The Ag doping level causes significant influence on the properties of the system prepared. The results indicated that 10.0 mol.% Ag doping causes major property improvements. The deposited films were characterized by their structural, morphological, surface smoothness, optical and gas sensitivity. The X-ray diffraction analysis shows the polycrystalline growth of $Cu_{2-x}Ag_xO$ films. The substitution by Ag^{2+} ions result in cubic structure (111) preferential orientation. The transmittance and optical band-gap values are maximum (≈2.12 to 1.73eV) for the Ag doping level of 10.0 mol.%. The Fourier transform infrared (FTIR) results confirmed the stretching vibrations of Cu-O and Ag-O. The Gas sensitivity revealed, Ag doped Cu_2O serve as sensor material for the detection of NH_3 molecules at room temperature compared to undoped film. The gas sensing test was performed by the resistance measurement of the system using a Keithley System.

Keywords: Silver (Ag) doped Cu_2O thin films, 3D Flower-like structure, Structural and Gas Sensitivity.

1. Introduction

In the search of a suitable p-type semiconductor, cuprous oxide (Cu_2O) appears to be one of the promising semiconductors for solar cells. Cu_2O based materials are especially useful for light emitting diodes [1]. Cuprous oxide is the parent compound of many p-type transparent conducting metals oxides (TCOs) such as Cu_xO_2delafossites (X= Ag, Zn, Fe, Co, Al, KCL, etc.) [2]. The property of the Cu_2O material can be enhanced with doping of Ag without affecting the crystal structures. Generally, metal doping materials are making radical changes in electrical, optical, morphological, magnetic properties, gas sensitivity and antibacterial activities of copper oxide thin films [3]. It is used in many applications which include photo catalyst [4-10], lithium-ion batteries [11], solar energy [12,13], magnetic semiconducting material [14], transparent conductors [15], water splitting [16-24] and gas sensors [25]. For the preparation of this material in thin film form, several deposition techniques are available such as chemical vapour deposition [26,27], thermal oxidation [28], hydrothermal deposition [29], electro thermal deposition [30], magnetic reactive sputtering [31], one step hydro thermal [32], chemical bath deposition(CBD) [33], epitaxial growth [34], Pulsed laser deposition [35-37], spray pyrolysis [38] and successive ionic layer adsorption and reaction method (SILAR) [39]. Among the various methods, the SILAR technique is a simple one, non-toxic with low processing temperature and also can lead to large area deposition. However, there are only a few reports available on the deposition of metal doped Cu_2O thin films by SILAR technique. Here, we have reported the deposition of Ag-doped Cu_2O films using SILAR method.

2. Experimental Procedure

Undoped and Ag doped Cu_2O (2.5, 5.0, 7.5 and 10.0 mol. %) films were deposited onto glass substrates using SILAR technique. High pure copper sulphate pentahydrate, sodium thiosulfate, silver nitrate and sodium hydroxide were used for preparing precursor solution. Then 2.5, 5.0, 7.5 and 10

*Corresponding author E-mail: dhana_pgp@rediffmail.com

mol. % of $AgNO_3$ was added to the precursors and stirred using a magnetic stirrer. The deposition cycle consists of three steps. (1). Immersion of substrate in hot NaOH (80 °C) solution for 20 s. (2). immersion in copper thiosulphate complex solution for 20 s. (3). Rinsing the substrate in deionized water bath for 10 s to remove the unreacted Cu^+ and OH^- ions and loosely bounded particles from the substrate. A schematic representation of the SILAR process is shown in Fig. 1. These three steps were repeated for 30 cycles for each sample. Fig (2) shows the deposited thin films onto glass substrates.

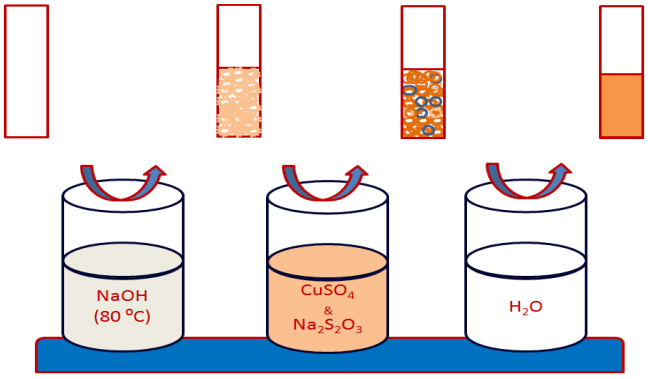

Fig. 1: A schematic representation of the SILAR method

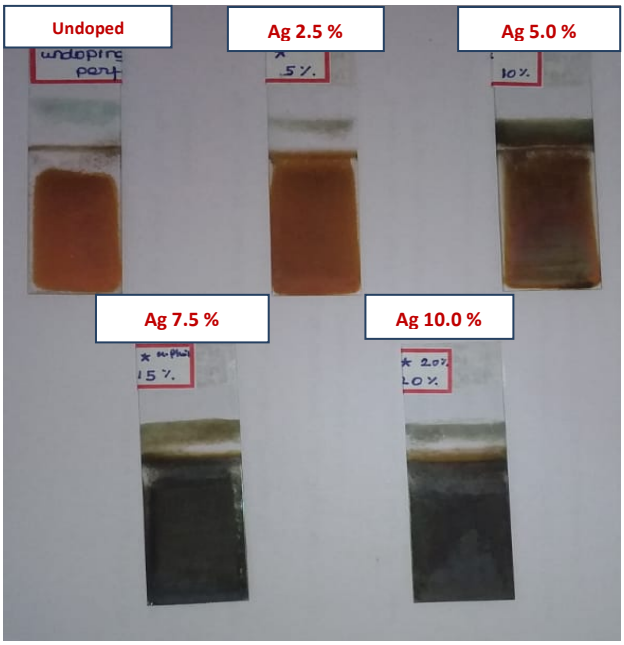

Fig. 2: Experimental image for the undoped and Ag doped Cu_2O thin film

3. Results and discussion

3.1 X-Ray diffraction analysis:

Fig. (3) shows the XRD pattern of undoped and silver (Ag) doped cuprous oxide (Cu_2O) thin films for different doping concentration levels. In the case of undoped film, there is only one peak at $2\theta = 36.35^0$ corresponding to the lattice plane (111) indicating that the deposited film is Cu_2O with cubic structure according to the JCPDS Card No: 05-0667. The intensity of undoped film is feeble. The low intensity of the diffraction peaks observed may be due to the presence of more Cu and O vacancies in the Cu_2O lattice plane. When the Ag is doped with the Cu_2O, the intensity of the peak is gradually increased, indicating the filling of vacancies. This means, when Ag is doped with Cu_2O lattice, the Cu^{2+} and O^{2-} ions may be settled at the Cu and O vacancies, improving the periodic alignment of crystal lattice. This result may be attributed to the lower binding energy between Ag and O (907.0 eV) [40] than that between Cu_2 and O (952.3 eV) [41]. When increasing the Ag doping level to 7.5 mol.%, the orientation plane of (111) is found to be the same (Cu_2O plane), however, there are additional diffraction peaks at $2\theta = 38.22^0$ and $2\theta = 44.32^0$ (JCPDS Card No: 40-1054) indicating the presence of the secondary phase. The corresponding planes are (022) and (032). When the maximum doping level of Ag (10.0 mol.%) was employed, the intensity of diffraction peaks of (111) and (022) planes suddenly increased (nearly three times). That means when the doping level is increased, the excess Ag ions take the interstitial positions of the crystal lattice. The diffraction pattern revealed sharp and high intensity peaks compared to undoped and other Ag doped ones. The observed result can be attributed to the improved crystalline quality of the film at higher doping levels.

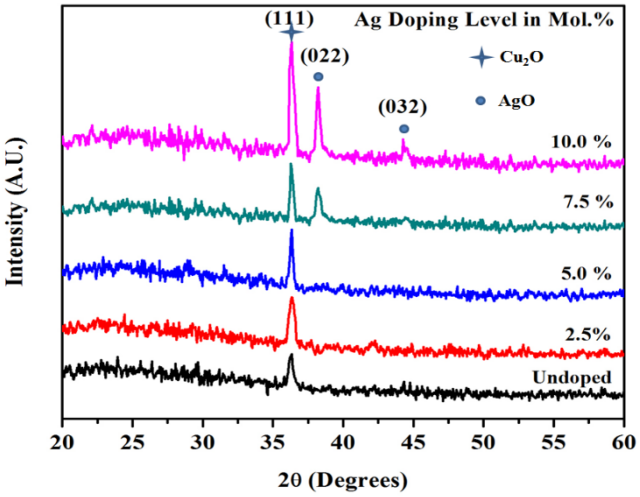

Fig. 3: XRD Patterns of undoped and Ag doped Cu_2O thin films

The observed shift of prominent peaks towards higher angles when doping adds evidence to the incorporation of Ag ions into the Cu sites and indicating the narrowing of 'd' spacing. As the ionic radius of Ag^{2+} (70 pm) is less than that of Cu^{2+} (77 pm), this reduction in the 'd' spacing is an expected result.

The average crystalline size was calculated using Debye-

Scherrer formula [42, 43] is,

$$D = \frac{k\lambda}{\beta \cos\theta} \quad (1)$$

The lattice parameter 'a' of the cubic system of Cu_2O film and dislocation density (δ)and micro strain (ε) are calculated using the following formula [44]. The values are given in Table.1.

Table 1: Structural and optical parameters of undoped Ag-doped Cu_2O thin films

S.No	Ag Doping level (Mol.%)	Crystallite size (D) nm	Lattice parameter (a) 10^{-1} nm	Dislocation Density(δ) $x10^{15}$ (lines/m^2)	Micro strain (ε) $x\ 10^{-3}$	Optical band gap (Eg) eV
1.	0	23.2447	4.3023	1.8507	1.4912	2.12
2.	2.5	27.4132	4.2862	1.2387	1.21998	2.04
3.	5.0	28.9887	4.2736	1.2857	1.2429	1.98
4.	7.5	42.0016	4.2830	0.85496	1.0135	1.82
5.	10.0	42.8923	4.2893	0.5436	0.8082	1.73

$$\frac{1}{d2} = \frac{h2+k2+l2}{a2} \quad (2)$$

$$\delta = \frac{1}{D2} \quad (3)$$

$$\delta = \frac{\beta \cos\theta}{4} \quad (4)$$

3.2 Optical Properties:

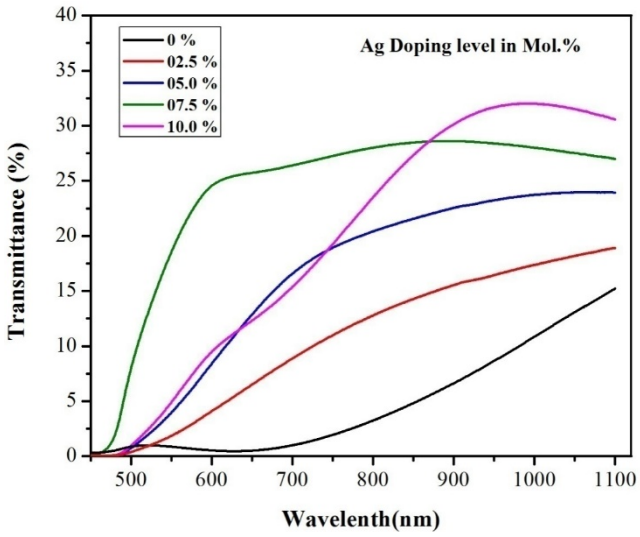

Fig. 4: UV-vis NIR transmittance spectrum of undoped and Ag doped Cu_2O thin films

Fig. (4) shows the optical transmittance spectra of undoped, and Ag doped films observed in the range of wavelengths 480 and 1100 nm. The transmittance of the undoped film is only nearly 15 % and gradually increases with the doping concentration. A maximum doping of Ag in to Cu_2O results in a higher transmittance of nearly 35 %. The gradual improvement of optical transmittance of the film may be due to the ability of the film surface to reduce reflectivity and diffuse scattering [45]. When the transmittance is high in the visible region, it is useful for aesthetic window glass materials. It's important to mention here that the sharpness of the absorption edge is high at the doping level of Ag 10 mol.% indicating better crystalline quality of the films when compared with other films as shown in Fig. (5). Fig (6) illustrates the E_g of the films found using Tauc's plot [46,47].

$$(\alpha h\nu)^2 = A\,(h\nu - E_g) \quad (5)$$

Where A and E_g are the constant and optical band gap respectively. The E_g can be determined by extrapolation of the linear portion of the curve to the hν axis. The band gap of the film decreases with an increase in doping level.

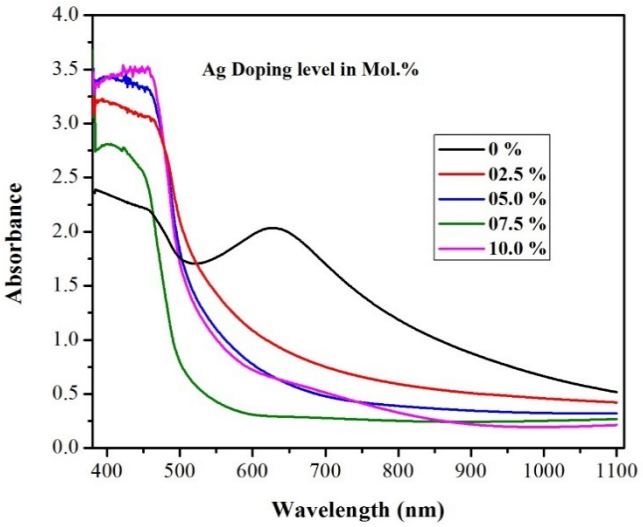

Fig. 5: UV-vis NIR absorbance spectrum of undoped and Ag doped Cu_2O thin films

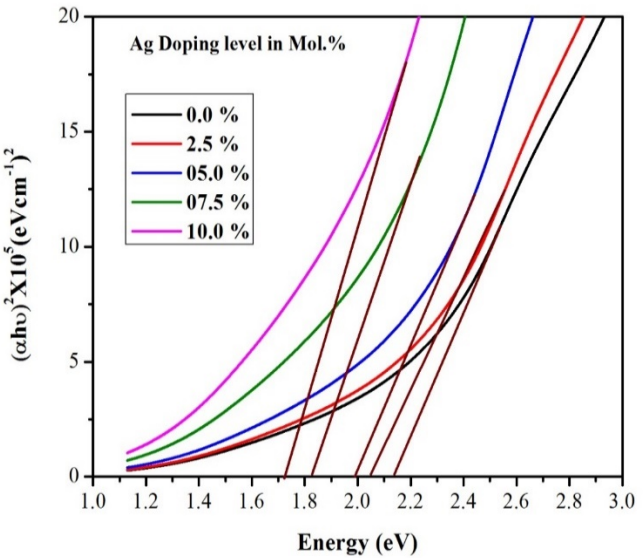

Fig. 6: $(\alpha h\nu)^2$ versus hν plots of undoped and Ag doped Cu_2O thin films

3.3 FTIR Studies:

Fig. (7) shows the Fourier transformation infrared (FTIR) spectra in the range 480 - 2000 cm^{-1}. Generally, FTIR spectrum of metal oxide exhibits absorption bands below 1000 cm^{-1} which arise owing to inter atomic vibrations [48]. The spectrum of undoped film exhibits minimum

absorption peak at 406 and 470 cm^{-1} related to stretching vibrations of Cu-O in the cuprous oxide film [49]. This minimum absorption peak obtained from undoped film reveals the poor crystalline quality. For the Ag doped (2.5 and 5.0 mol. %.) Cu_2O lattice, absorption peaks are observed at 448, 521 & 446, 561 cm^{-1}. Now additional absorption peaks are revealed at 690 cm^{-1} and 688 cm^{-1}corresponding to the doping level, indicating the stretching mode of Ag-O bonds [50]. Further increase in the doping level produced increase in the intensity of the absorption peaks of Cu-O and Ag-O. Moreover, the peak at 618 cm^{-1} is attributed to the formation of Cu_2O [51]. The broad band absorptions between the range of 1300 and 2000 cm^{-1} are revealed indicating the presence of H_2O and CO_2 molecules.

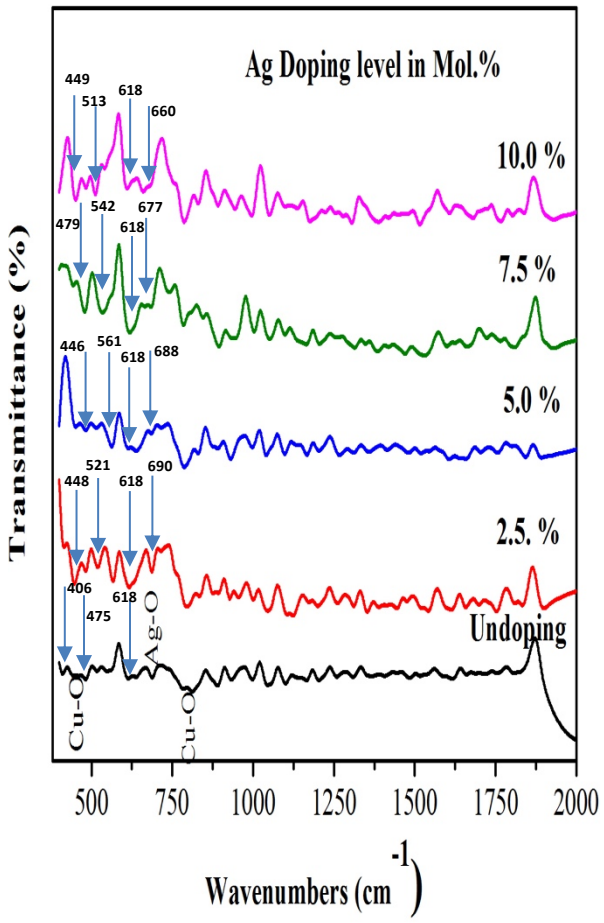

Fig. 7: FTIR spectra of undoped and Ag doped Cu_2O thin films

3.4 Photoluminescence:

Fig. (8) shows the photoluminescence (PL) spectra of the films (Ag = 2.5, 5.0, 7.5 and 10.0 mol.%). The PL spectra are usually used to study electron- hole recombination. All the films exhibit two peaks nearly at wavelengths 549 and 610 nm. The near band emission (NBE) peaks appear at 549 nm [52]. The peak intensity increases with the increase of Ag doping level. That means the doped ions (Ag^{2+}) are settled in to the Cu^{2+} and O^{2-} vacancies. It can be attributed to the crystalline quality of the film that is improved when a maximum doping level of Ag is employed. Also, the peaks shift to lower wavelengths with the increase of doping concentration. The blue-shift observed is attributed to Burstein-Moss effect of the nanosized particle [53]. This result is correlated with XRD inferences.

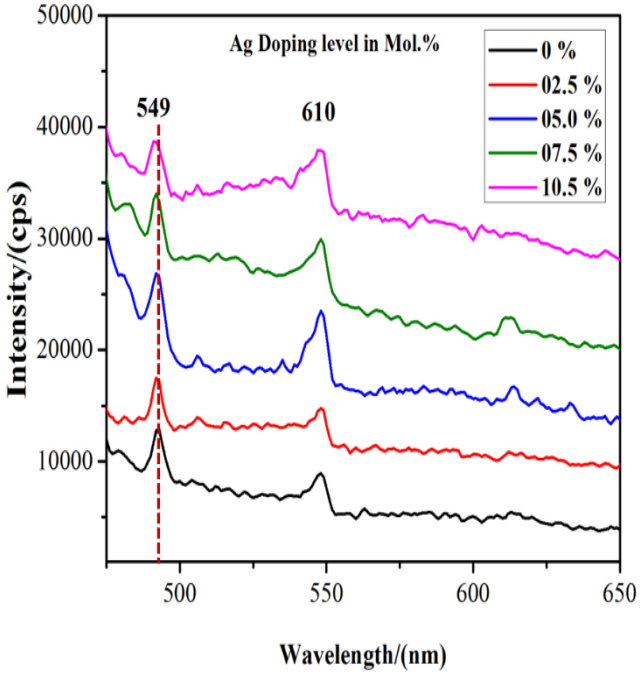

Fig. 8: Photoluminescence spectra of undoped and Ag doped Cu_2O thin films

3.5 Field Emission Scanning Electron Microscope (FESEM):

Fig. (9) shows the FESEM of thin films. The proportion of reactive compounds markedly affects the size and morphology of the deposited thin films. In the surface micrographs of undoped film, a large number of small particles are found agglomerated, due to Van-der walls force as shown in fig. (9-a) [54]. The small particles combine to form a large grain with different nanoscales. From fig.(9-b), (2.5 % Ag doping), it is clearly seen that the shape and size of the grains are altered with the doping of silver (2.5 mol.%). Additionally, perfect and bigger rod-like structures are revealed with different lengths and breaths. It is one piece of evidence for the influence of doped compounds which change the surface morphology. In Fig. (9-c) the micrograph obtained when the doping level is increased (5.0 mol.%) is presented. All the grains and bigger rod-like structures disappeared and revealed the formation of number of small rod-like grains scattered in all

directions and agglomerated. For 7.5 mol.% Ag doping, small rod-like structures disappeared and exhibit the number of grains like structure and some nano-rods like structures got agglomerated. With increasing doping level, the initially formed Cu_2O nuclei are assembled, forming individual flowers but clear petals are invisible and finally for (Ag = 10. Mol.%) number of 3D flower-like structures revealed petals clearly. From the visible inspection of the surface morphology improved morphology for the films grown at higher Ag doped Cu_2O thin films can be ascertained.

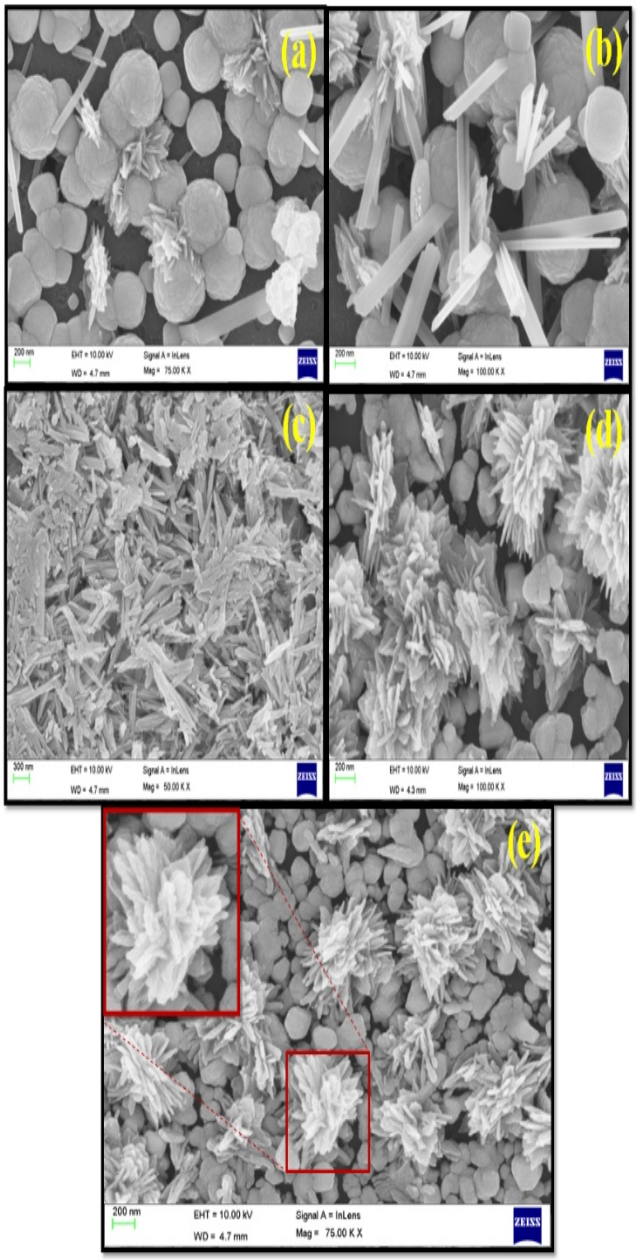

Fig. 9: FESEM images of undoped and Ag doped Cu_2O thin films

3.6 TEM, HRTEM and SEAD Pattern analysis:

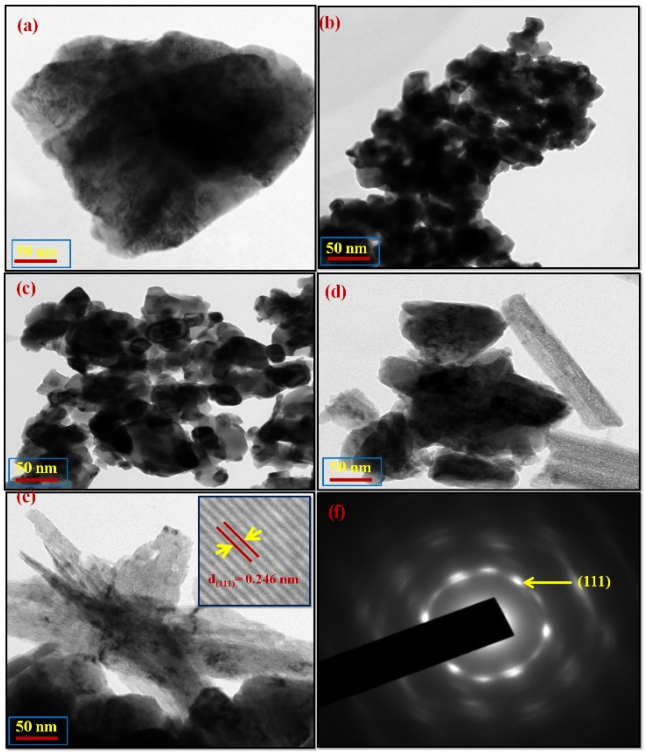

Fig. 10: TEM and HRTEM images of undoped and Ag doped Cu_2O thin films, (a). Undoped Cu_2O (b). Ag:2.5 %, (c). Ag:5.0 %, (d). Ag: 7.5%, (e). Ag: 10.0 % (HRTEM Image Inset), (f). SEAD Pattern image of Ag doped 10.0 mol %

Fig. (10) shows the TEM, HRTEM and SAED pattern images of undoped and Ag doped (Ag = 2.5, 5.0, 7.5 and 10.0 mol.%) Cu_2O thin films respectively. The TEM images are consistent with FESEM results. The deposition of undoped film, its achieved surface grains are apt to agglomerate in the single point like a diamond structure as shown in fig. (10-a). The doping of Ag further increases, and the particles are scattered as shown in fig. (10-b &c). That means, it has been extensively investigated to improve the separation of the grains through the applications of some external energy added by increasing doping concentration. Fig. (10-d) exhibit nano-rod like structure formation. For maximum doping level of Ag concentration, all the nano-rod disappears and appears to form a leaf-like structure as shown in fig. (10-e). The HR-TEM images of the films depict the growth along the (111) the plane. The fringe spacing is measured to be approximately 0.246 nm which is related to (111) lattice plane of the cubic Cu_2O. The 'd' spacing corresponds to (111) plane (JCPDS Card No: 05-0667). The SAED pattern reveals that the entire structure of ellipsoid is a single crystal with the preferential

orientation growth of (111). The SAED pattern of TEM image (Ag doped with 10.0 mol.%.) is presented in fig. (10-f). This result implies that the subunits are oriented in (!1111) plane assemble with each other and finally forme a larger grain with a single crystal structure.

3.7 Atomic Force Microscope (AFM) analyses:

Fig. (11 & 12) show the three-dimensional AFM images of 10 μm^2 of the crystallized undoped and Ag doped (10.0 mol. %) Cu_2O thin films to grow on glass substrate. The undoped surface relief show roughness and shaped crystallites. It is observed that the cluster size decreases slightly and is quite smooth compared to undoped film. This is due to the uniform distribution of the Ag doped thin films. We can conclude that the Ag doped (10.0 mol.%) film is the optimum value to the Cu_2O deposition film. This is in agreement with XRD, FESEM and HRTEM analysis.

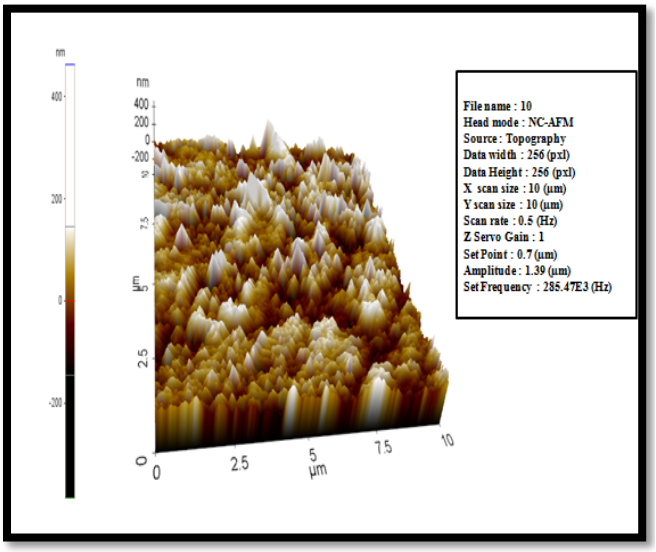

Fig. 11: 3D AFM images for crystallized undoped Cu_2O thin films grown on glass substrate

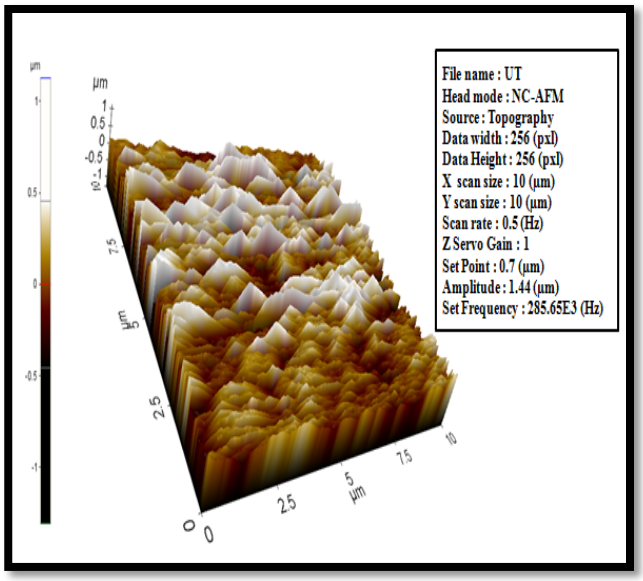

Fig. 12: 3D AFM images for crystallized Ag (10.0 mol.%) doped Cu_2O thin films grown on glass substrate

3.8 Ammonia gases sensing:

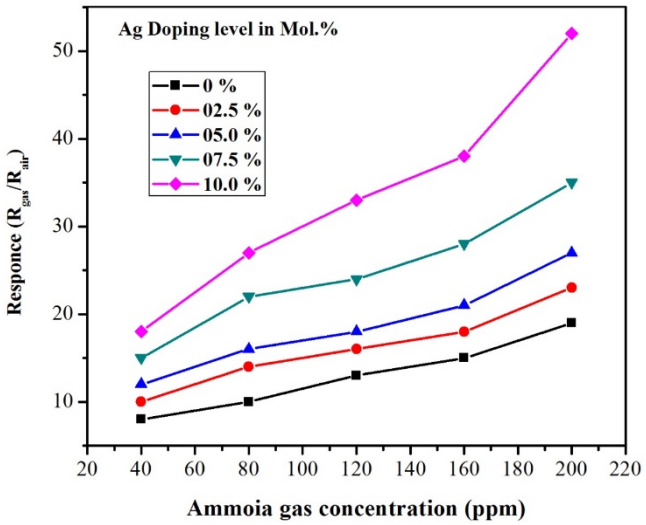

Fig. 13: Response values of un doped and Ag doped Cu_2O thin films to ammonia gas at room Temperature

For metal oxide semiconductor gas sensing materials, doping of noble metals can improve the sensing ability. The probable metals include Ag [55], Au [56], Pd [57] and Pt [58]. Fig. (13) show the room temperature (303 K) ammonia gas sensitivity of undoped Ag doped (Ag= 10.0 mol.%) Cu_2O thin films. The gas sensing test were performed by the resistance measured for the system with and without gas ambience. The ammonia gas used was pure (without any contents of other gases). A comparative response of Ag doped Cu_2O thin films with reference to pure in the presence of 50 ppm of ammonia vapour were studied. Ag doped film showed better response than the undoped film. High density of dangling bonds (Cu^{2+}) and

unsaturated oxygen coordinate generally causes good gas adsorption. This might be due to the enhanced oxygen adsorption on the Cu_2O surface caused by the dopant Ag atoms and the associated increase in the base resistance of the film [59]. Since ammonia vapour is a reducing gas, an enhanced or sharp decrease of surface resistance from a higher to lower value was observed for doped film when compared with the undoped. This trend was strongly supported by the increasing trends of response with increasing Ag-dopant concentration.

4. Conclusion

Undoped and Ag doped Cu_2O films were deposited onto glass substrate using a low-cost SILAR technique. All the films were characterized by XRD, UV-vis NIR, FTIR, PL, FESEM, HRTEM, AFM and Gas Sensitivity. Through the XRD, the structural properties were investigated for all the films, and the films maintain the preferred (111) plane orientation at the same time the doping of Ag (7.5 and 10.0 mol.%) revealed few peaks of AgO at the plane of (022) and (032). The crystalline size varied from 23.24 to 42.89 nm. It's found that film doped with 10.0 mol. % of Ag concentration has better optical transmittance (≈ 35%) and decreased optical band gap. The surface morphology of the films was investigated using FESEM. From HR-TEM analysis revealed that the Ag doped (10.0 mol.%) Cu_2O thin film predominantly possess (111) crystal plane. AFM studies revealed that the smoothness of the film increased when maximum doping of Ag concentration. The increases of ammonia gas sensitivity for Ag doped Cu_2O film (Ag=10.0 mol.%) compare than undoped film.

References:

[1] L. C. Chen Review of preparation and optoelectronic characteristics of Cu_2O-based solar cells with nanostructure Materials Science in Semiconductor Processing, *Mater. Sci. Semicond. Process*. **16,** 1172-1185 (2013).

[2] L. Zhang, L. McMillon, J. McNatt, Gas-dependent band gap and electrical conductivity of Cu_2O thin films, *Sol. Energy Mater. Sol. Cells.* **108,** 230 -234 (2013).

[3] F. Bayansal, T. Tas Ko Pru, B. Sahin, H.A. Cetinkara, Effect of cobalt doping on nano structured CuO thin films, *Metall. Mater. Trans. A*, **45**, 3670-3674 (2014).

[4] J.M.D. Coey, M. Venkatesan *C.B. Fitzgerald, Donor impurity band exchange in dilute ferromagnetic oxides Nat. Mater.***4,** 173 - 179 (2005).

[5] Y. Ghayeb, M.M. Momeni, A. Mozafari, Effect of silver sulfide decorating on structural, optical and photocalatalytic properties of iron-doped titanium dioxide nanotubes films, *J. Mater. Sci. Mater. Electron* doi:10.1007/s10854-016-5321-8

[6] M.M. Momeni, One-step synthesis of ZnO nanowires on zincfoils and their photocatalytic properties, *Indian J. Chem.*55A, 686-691 (2016)

[7] M.M. Momeni, I. Ahadzadeh, Copper photodeposition on titania nano tube arrays and study of their optical and photocatalytic properties *Mater.Res. Innov.***20**, 44-50 (2016).

[8] M.M. Momeni, Y. Ghayeb, Z. Ghonchegi, Fabrication and characterization of copper doped TiO_2 nanotube arrays by in situ electrochemical method as efficient visible-light photocatalyst, *Ceram. Int.***41,** 8735 – 8741(2005).

[9] M.M. Momeni, M. Mirhosseini, M. Chavoshi, A. Hakimizade, The effect of anodizing voltage on morphology and photocatalytic activity of tantalum oxide nanostructure, *J.Mater. Sci. Mater. Electron.* **27,** 3941-3947 (2016).

[10] M.M. Momeni, M. Hakimian, A. Kazempour, . In-situ manganese doping of TiO_2 nanostructures via single-step electrochemical anodizing of titanium in an electrolyte containing potassium permanganate: a good visible-light, *Ceram. Int.***41,** 13692-13701 (2015).

[11] X.P. Gao, J.L. Bao, G.L. Pan, H.Y. Zhu, P.X. Huang, F. Wu, D.Y. Song Preparation and electrochemical performance of polycrystalline and single crystalline CuO nanorods as anode materials for Li ion battery. *J. Phys. Chem. B* **108**, 5547–5551 (2004).

[12] V. Georgieva, M. Ristov, Electrodeposited cuprous oxide on indium tin oxide for solar applications, *Sol. Energy Mater. Sol. Cells,***73,** 67 – 73 (2002).

[13] K. Han, M. Tao, Electrochemically deposited-n homojunction cuprous oxide solar cells *Sol. Energy Mater. Sol. Cells* **93,** 153 -157 (2009).

[14] S.N. Kale, S.B. Ogale, S.R. Shinde, M. Sahasrabuddhe, V. Kulkarni, R. Greene, T. Venkatesan, Magnetism in cobalt-doped Cu_2O thin films withut and with Al,Vor Zn codopants, *Appl. Phys. Lett.***82,** 2100 -2104 (2003).

[15] M. Beekmana, J. Salvadorb, X. Shic, G.S. Nolasa, J. Yangb, Characterization of delafossite-type $CuCoO_2$ prepared by ion exchange, *J. Alloys Compd.***489,** 336-338 (2010).

[16] P.E. de Jongh, D. Vanmaekelbergh, J.J. Kelly, Cu_2O: a catalyst for the photochemical decomposition of water?, *Chem. Commun.***12,** 1069 –1070 (1999).

[17] T.-L. Li, Y.-L. Lee, H. Teng, High-performance quantum dot-sensitized solar cells based on sensitization with $CuInS_2$ quantum dots/CdS heterostructure, J. *Energy Environ. Sci.***5,** 5315 – 5324 (2012).

[18] H.Y. Xu, C. Chen, L. Xu, J.K. Dong, Direct growth and shape control of Cu_2O film via one-step chemical bath deposition, *Thin Solid Films.* **527,** 76-80 (2013).

[19] M.M. Momeni, Y. Ghayeb. Photoinduced deposition of gold nanoparticles on TiO_2–WO_3 nanotube films as efficient photoanodes for solar water splitting, *Appl. Phys. A***122** 1 – 10 (2016).

[20] M.M. Momeni, M. Hakimian, A. Kazempour, Preparation and characterisation of manganese–TiO_2 nanocomposites for solar water splitting, *Surf. Eng.***32,** 514-519 (2016).

[21] M.M. Momeni, Y. Ghayeb, M. Davarzadeh, Photoelectrochemical water splitting on chromium-doped titanium dioxide nanotube photoanodes prepared by single-step anodizing, *J. Alloys Compd.* **637,** 393-400 (2015).

[22] M.M. Momeni, Y. Ghayeb Fabrication, characterization and photoelectrochemical performance of chromium-sensitized titania nanotubes as efficient photoanodes for solar water splitting, *J. Solid State Electrochem.* **20,** 683-689 (2016).

[23] M.M. Momeni, Y. Ghayeb Cobalt modified tungsten–titania nanotube composite photoanodes for photoelectrochemical solar water splitting, *J. Mater. Sci. Mater. Electron.* **27,** 3318-3327 (2016).

[24] M.M. Momeni Highly efficient photoelectrochemical water splitting by a novel nanocomposite titania photoanode, *Mater. Res. Innov.* **20 (4),** 317-325 (2016).

[25] P.A. Praveenjanantha, L.N.L. Perera, K.M.D.C. Jayathilaka, J.K.D.S. Jayanetti, D.P. Dissanayaka, W.P. Siripala, Use of Cu_2O microcrystalline thin film semiconductors for gas sensing, Proceedings of the Technical Sessions, **25**, 70-76 (2009).

[26] V.P. Godbole, R.D. Vispute, S.M. Chaudhari, S.M. Kanetkar, S.B. Ogale Dependence of the properties of laser deposited tin oxide films on process variables *J. Mater. Res.***5,** 372 -377 (1990).

[27] R.K. Singh, J. Naraya Pulsed-laser evaporation technique for deposition of thin films: Physics and theoretical model, *Phys. Rev. B***41,** 8843- 8862 (1990).

[28] M. Vila, C. Dı´az-Guerra, J. Piqueras, Optical and magnetic properties of CuO nanowires grown by thermal oxidation *J. Phys. D : Appl. Phys.* **43,** 135403 – 135409 (2010).

[29] Q. Zhang, W. Fan, L. Gao, Anatase TiO_2 nanoparticles immobilized on ZnO tetrapods as a highly efficient and easily recyclable photocatalyst, *Appl. Catal. B* **76,** 168-173 (2007).

[30] X. Yu, X. Li, G. Zheng, Y. Wei, A. Zhang, B. Yao, Preparation and properties of KCl-doped Cu_2O thin film by electrodeposition, *Appl. Surf. Sci.* **270,** 340 – 345 (2013).

[31] K. Akimoto, S. Ishizuka, M. Yanagita, Y. Nawa, G.K. Paul, T. Sakurai, Thin film deposition of Cu_2O and application for solar cells, *Sol. Energy,* **80,** 715-722 (2006).

[32] M.M. Momeni, M. Mirhosseini, M. Chavoshi Growth and characterization of Ta_2O_5 nanorod and WTa_2O_5 nanowire films on the tantalum substrates by a facile one-step hydrothermal method, *Ceram. Int.* **42,** 9133-9138 (2016).

[33] A. Vasuhi, R. John Xavier, R. Chandramohan, S. Muthukumaran, K. Dhanabalan, M. Ashokkumar & P. Parameswaran, Effect of heat-treatment on the structural and optical properties of Cu_2S thin films deposited by CBD method *J Mater Sci: Mater Electron* DOI 10.1007/s10854-013-1652-x

[34] A. Catana, J.P. Locquet, S.M. Paik, I.K. Schuller Local epitaxial growth of CuO films on MgO, *Phys. Rev. B* **46,** 15477 -15483 (1992).

[35] A. Chen, G. Yang, H. Long, F. Li, Y. Li, P. Lu Nonlinear optical properties of laser deposited CuO thin films, *Thin Solid Films,* **517,** 4277 – 4277 (2008).

[36] S.B. Ogale, P.G. Bilurkar, N. Mate, S.M. Kanetkar, N. Parikh, B. Patnaik, Deposition of copper oxide thin films on different substrates by pulsed excimer laser ablation, *J. Appl. Phys.* **27,** 3765- 3769 (1992).

[37] N. Kikuchi, K. Tonooka, Electrical and structural properties of Ni-doped Cu_2O films prepared by pulsed laser deposition, *Thin Solid Films,* **486,** 33- 37 (2005).

[38] N.J. Begum, R. Mohan, K. Ravichandran, Effect of solvent volume on the physical properties of aluminium doped nanocrystalline zinc oxide thin films deposited using a simplified spray pyrolysis technique, *Super Lattice Microstruct.* **53,** 89-98 (2013).

[39] A. T. Ravichandran, K. Dhanabalan, S. Valanarasu, A. Vasuhi, A. Kathalingam, Role of immersion time on the properties of SILAR deposited CuO thin films, *J Mater Sci: Mater Electron* DOI 10.1007/s10854-014-2483-0.

[40] D.R. Patil, L.A. Patil, P.P. Patil Cr_2O_3-activated ZnO thick film resistors for ammonia gas sensing operable at room temperature, *Sens. Actuators B: Chem.***126,** 368-374 (2007).

[41] M. Aslam, V.A. Chaudhary, I.S. Mulla, S.R. Sainkar, A.B. Mandale, A.A. Belhekar, K. Vijaymohan, A highly selective ammonia gas sensor using surface ruthenated zinc oxide, *Sens. Actuators*, A75, 162-167 (1999).

[42] A.T. Ravichandran, K. Dhanabalan, A. Vasuhi, R. Chandramohan, and Srinivas Mantha, Morphology, bandgap and grain size tailoring in Cu_2O thin film by SILAR method, *IEEE Transactions on Nanotechnology,* **14,** 105-112 (2015).

[43] S. Satheeskumar, S. Vadivel, K. Dhanabalan, A. Vasuhi, A. T. Ravichandran, K. Ravichandran, Enhancing the structural, optical and magnetic properties of Cu_2O films deposited using a SILAR technique through Fe doping, , *J Mater Sci: Mater Electron*, https://doi.org/10.1007/s10854-018-8966-7.

[44] K. Dhanabalan, A. T. Ravichandran, K. Ravichandran, S. Valanarasu, Srinivas Mantha, Effect of Co doped material on the structural, optical and magnetic properties of Cu_2O thin films by SILAR technique, *J Mater Sci: Mater Electron* DOI 10.1007/s10854-016-6072-2.

[45] K. Ramamoorthy, C. Sanjeeviraja, M. Jayachandran, K. Sankaranarayanan, P. Misra, L.M. Kukreja, Development of a novel high optical quality ZnO thin films by PLD for III–V opto-electronic devices, *Curr. Appl. Phys.* **6,** 103–108 (2006).

[46] P.-H. Hsieh, Y.-M. Lu, W.-S. Hwang, J.-J. Yeh, W.-L. Jang Effect of Al content on electrical conductivity and transparency of P-type Cu-Al-O thin film, *Surf. Coat. Technol.* **205,** S206 –S209 (2010).

[47] Srinivas Mantha, A. T. Ravichandran, K. Dhanabalan, A. Vasuhi Dhanabalan, R. Chandramohan, *Morphology, bandgap and grain size tailoring in Cu_2O thin film by modified chemical bath deposition technique and methods employed thereof,* Indian Patent **321095**, Sep. 23, (2019).

[48] M.F. Khan, A.H. Ansari, M. Hameedullah, E. Ahmad, F.M. Husain, Q. Zia, U. Baig, M.R. Zaheer, M.M. Alam, A.M. Khan, Z.A. Alothman, I. Ahmad, G.M. Ashraf, G. Aliev, Sol-Gel Synthesis of Thorn-Like ZnO Nanoparticles Endorsing Mechanical Stirring Effect and Their Antimicrobial Activities: Potential Role as Nano-Antibiotics, *Sci Rep*. **6,** 1-12 (2016).

[49] I.Y. Erdogan, O. Gullu, Optical and structural properties of CuO nanofilm: Its diode application *J. Alloys Compd.***492,** 378 – 383 (2010).

[50] S. Rafique, A. K. Kasi, J. K. Kasi, Aminullah, M. Bokhari, and Z. Shakoor, Fabrication of silver-doped zinc oxide nanorods piezoelectric nanogenerator on cotton fabric to utilize and optimize the charging system, *Nanomater. Nanotechnol.*, **10,** 1–12 (2019).

[51] N. Ekthammathat, T. Thongtem, S. Thongtem, Antimicrobial activities of CuO films deposited on Cu foils by solution chemistry, *Appl. Surf. Sci.* **277,** 211-217 (2013).

[52] A. T. Ravichandran, K. Dhanabalan, K. Ravichandran, R. Mohan, K. Karthika, A. Vasuhi, B. Muralidharan, Tuning the structural and optical properties of SILR deoisited Cu_2O films through Zn doping, *Acta Metall. Sin. (Engl. Lett.),* DOI 10.1007/s40195-015-0292-y.

[53] K. Mageshwari, R. Sathyamoorthy, Physical properties of nanocrystalline CuO thin films prepared by the SILAR method, *Mater. Sci. Semicond. Process.***16,** 337–343 (2013).

[54] K. Maaz, A. Mumtaz, S.K. Hasanian, A. Ceylan, Synthesis and magnetic properties of cobalt ferrite ($CoFe_2O4$) nanoparticles prepared by wet chemical route, *J. Magn. Magn. Mater.* **308,** 289-295 (2007).

[55] Y. Wei, X. Wang, G. Yi, L. Zhou, J. Cao, G. Sun, Z. Chen, H. Bala and Z. Zhang, Hydrothermal synthesis of Ag modified ZnO nanorods and their enhanced ethanol-sensing properties. *Mater. Sci. Semicond. Process.***75,** 327–333 (2017).

[56] S. M. Yousefi, S. Rahbarpour and H. Ghafoorifard, Describing the effect of Ag/Au modification on operating temperature and gas sensing properties of thick film SnO_2 gas sensors by gas diffusion theory, *J. Mater. Chem. Phys.* **227,** 148-156 (2019).

[57] Jin-Young Kim, Jae-Hyoung Lee, Jae-Hun Kim, Ali Mirzaei, Hyoun Woo Kim, Sang Sub Kim, Realization of H2S sensing by Pd-functionalized networked CuO nanowires in self-heating mode, *Sens. Actuators.B.,* **299,** 126965- 126976 (2019).

[58] D. S. Dhawale, T. P. Gujar and C. D. Lokhande TiO_2 nanorods decorated with Pd nanoparticles for enhanced liquefied petroleum gas sensing performance, *Anal. Chem,* **89,** 8531-8537 (2017).

[59] S.T. Shishiyanu, T.S. Shishiyanu, O.I. Lupan, Novel NO_2 gas sensor based on cuprous oxide thin films, *Sensors and Actuators B chem.,* **113,** 468–476 (2006).